

# Steel Conduit and EMT Enclosed Circuits: Analysis and Testing

A.P.Sakis Meliopoulos, *Fellow, IEEE*, George Cokkinides, *Member, IEEE*  
School of Electrical and Computer Engineering  
Georgia Institute of Technology, Atlanta, Georgia 30332  
E-mail: sakis.m@gatech.edu

Joseph Andre  
Steel Tube Institute  
Bothell, WA 98012  
E-mail: jandre@steeltubeinstitute.org

**Abstract**—The performance of electric circuits enclosed in steel conduit or EMT is of great importance for the proper operation of industrial and commercial installations as well as the safety of humans in these facilities. This paper presents a comprehensive modeling procedure for these systems and the verification of these models with extensive testing under various loading conditions. The paper presents the mathematics of the approach as well as the testing procedure, test results and verification of the mathematical model. One important parameter in the model is the magnetization characteristics of the various steel raceway materials. The paper presents an elegant and simple procedure to measure the magnetic properties of the various raceway materials. The validated model is used to compute important design parameters, such as maximum permissible lengths and to assess the performance of specific designs. This work updates the results obtained with a similar but less comprehensive previous approach for modeling these systems.

**Index Terms**— Steel raceway, EMT, IMC, RMC, Stainless Steel, conductor segmentation, magnetic saturation, EGC.

## I. INTRODUCTION

Steel conduit and Electrical Metallic Tubing (EMT) are widely used as raceways for distribution of electrical power. For typical designs, the steel conduit or EMT does not carry any appreciable electric current under normal operating conditions. Under fault conditions, the steel conduit or EMT can be part of the fault current return path to the source, or it may be the only return path (by design) of the fault current to the source. The return path must have low enough impedance to allow fault current to quickly and safely operate protective devices. A relevant issue is that of grounding of steel conduit and EMT. During faults, the steel conduit or EMT could be elevated to a higher potential, which may or may not be hazardous. Appropriate grounding and bonding can and should be used to minimize the raceway voltage rise during faults. Performance evaluation of steel conduit and EMT relative to these problems requires exact modeling and testing of steel raceway systems under various excitation and fault conditions. This paper contains the results of a research project, which addressed the mentioned issues. Specifically, the paper addresses three fundamental issues associated with the use of steel conduit and EMT in secondary power distribution systems: (1) are steel conduit and EMT suitable equipment grounding conductors (EGC) with low enough impedance that enables good fault interruption and safety performance?, (2) what is the relative performance of other return paths, such as supplemental ground wires used in steel

enclosed secondary power systems? and (3) what is the ground potential rise of steel conduit and EMT during faults?

The paper is organized as follows. First, modeling of steel-raceway-enclosed single and multi-conductor systems is addressed. Next, full-scale tests for validating the model are described. The test results are presented and compared to the model prediction. Confirmation is very good. Next a number of applications are described with representative results: steel saturation levels, maximum allowable length, effects of electric current magnitude on raceway impedance, and raceway voltage elevation (GPR) under fault conditions. Finally the paper concludes with a summary and discussion.

## II. MODELING OF STEEL - RACEWAY--ENCLOSED POWER DISTRIBUTION SYSTEMS

A conceptual description of raceway-enclosed secondary distribution systems is illustrated in Fig. 1. We focus on one circuit, which may be connected, and be part of a larger electric installation with sources, transformers, loads, etc. Of special interest is the case of steel as a raceway because steel saturates resulting in a non-linear behavior of the circuit. In this paper, we focus on modeling the steel-raceway-enclosed system and the integration of this model to a general network analysis method. Modeling of the other components in the network is addressed elsewhere [1], [6]–[8], [11]. Specifically, we focus on: (1) characterization of the steel raceway material and (2) modeling of the steel-raceway-enclosed secondary distribution system conductors.

### A. Copper, Aluminum and Steel Material Characterization

The objective of characterization of the steel raceway material is to define the parameters of the steel raceway (resistivity and permeability) as functions of magnetic field and temperature. The resistivity as a function of temperature is given in terms of the resistivity at 20 degrees Celsius, the temperature and a coefficient alpha as shown in the equation:

$$\rho = \rho_{20^{\circ}C} (1 + \alpha(T - 20^{\circ}C)).$$

These parameters are measured with well-established measurement techniques and they are available (tabulated) for all the materials involved in raceway-enclosed circuits: copper, aluminum, steel and their alloys.

The permeability of copper and aluminum is also known and constant, approximately equal to the permeability of free space. The permeability of steel and its alloys can vary widely and it is dependent on the density of the magnetic field in the

material. For this reason, it is important to measure the permeability and establish the model of permeability for each specific steel alloy as a function of magnetic field density. We have developed a simple measurement method to extract the permeability properties of saturable conduit material and it is described in Appendix A. The method requires short samples of raceway and appropriate excitation and measurement equipment and provides the magnetization curve of the raceway material.

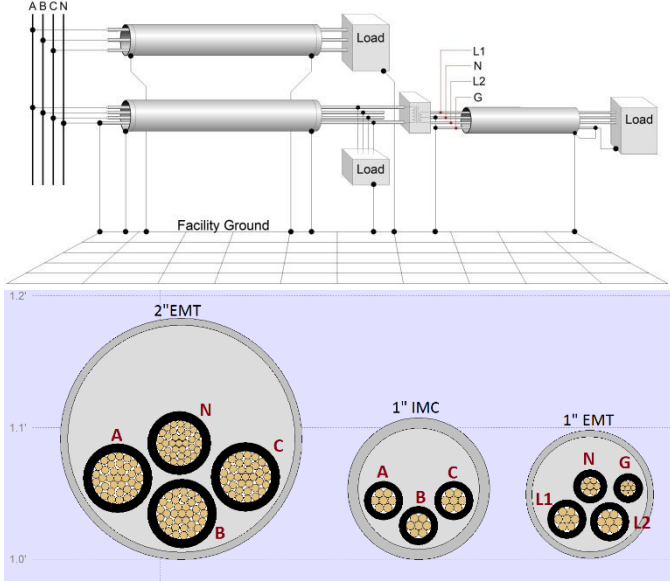


Figure 1: Raceway Enclosed Electric Circuits

### B. Single-Conductor Steel Raceway

In reference [1], the authors presented a single circuit analysis method for a steel raceway enclosed circuit by segmenting the raceway and conductors into cylindrical “pie” elements as shown in Figure 2 (left image). Subsequently, equations for the self-impedance of each element and the mutual impedances among all elements are developed and solved to determine voltages, currents, magnetic field density and impedances of all steel enclosed circuit components. This method works well for symmetrical configurations, such as the ones encountered in single steel enclosed circuits. For a general geometry the saturation analysis is approximate. For example in the case of two parallel steel raceway enclosed circuits the proximity effects are not accurately captured.

To overcome the limitations of the work presented in [1], we present here a new method that is able to accurately analyze non-symmetrical (user defined arbitrary configuration) steel raceway circuits, including circuits in close proximity. The method is based on triangular discretization. The entire space within the raceway-enclosed circuit, as well as the surrounding area (soil or free space) is discretized into a set of triangular elements. Conductors and steel are modeled in exact physical detail. Figure 2 (right image) illustrates a triangulation of a typical steel raceway enclosed circuit with two insulated copper conductors. A zoomed-in view of the triangular elements is shown in Figure 3.

The electric and magnetic fields in a cross-section of the circuit are computed using the equations governing the electric potential  $\phi$  and magnetic potential  $A_z$ :

$$-\frac{\partial}{\partial x} \left( \epsilon_r \frac{\partial \phi}{\partial x} \right) - \frac{\partial}{\partial y} \left( \epsilon_r \frac{\partial \phi}{\partial y} \right) = \rho_c / \epsilon_0, \quad -\frac{\partial}{\partial x} \left( \frac{1}{\mu_r} \frac{\partial A_z}{\partial x} \right) - \frac{\partial}{\partial y} \left( \frac{1}{\mu_r} \frac{\partial A_z}{\partial y} \right) = \mu_0 J_z$$

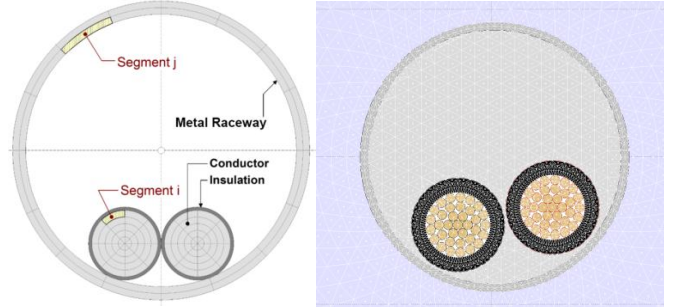


Figure 2: Cylindrical and Triangular Discretization Example

Using the triangular discretization, discrete values of the scalar and magnetic potential are assigned at each node of the triangles; assuming the potentials vary linearly within each discretization triangle, any field quantity anywhere in the triangle is expressed in terms of the potentials at the three vertices of each triangle (see Figure 3). The solutions for both the electric and magnetic potentials are formulated based on the well-known Ritz method (see reference [2]).

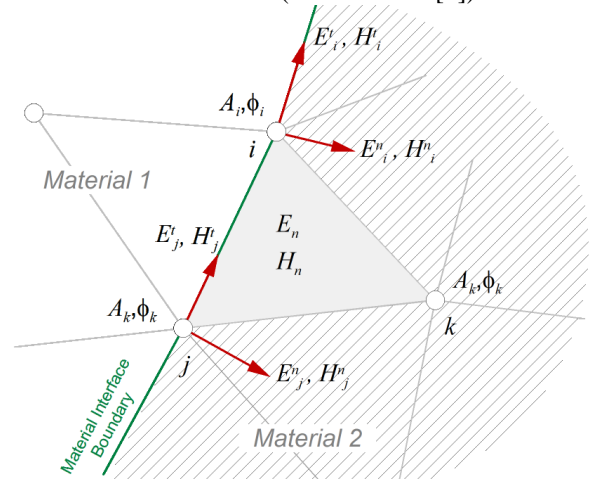


Figure 3: Elementary Triangle Field Vectors

Once the potentials at each discretization vertex is known, the electric field intensity  $E$  and magnetic flux density  $B$  are computed within each triangle using the equations:

$$\mathbf{B} = \nabla \times (A_z \hat{\mathbf{z}}) \quad \text{and} \quad \mathbf{E} = -\nabla \phi$$

Where:  $\phi$  : electric potential and  $A_z$  : magnetic potential.

Note that since it is assumed that the potentials vary linearly across each triangle, the electric and magnetic fields are constant within each triangle. The electric and magnetic field vectors at each triangulation vertex are computed by averaging the contributions of all triangles containing the vertex. However, if a vertex is on a material interface boundary (as vertices  $i$  and  $j$  in Figure 4) the averaging is performed by observing continuity conditions. Specifically, the vertex electric and magnetic fields are decomposed in components, which are normal and tangential to the boundary.

Given that the continuity holds for the tangential field vectors  $E^t$  and  $H^t$ , and the normal field vectors flux density  $D^n$ , and  $B^n$ , the continuous components are computed by averaging the contributions from both sides of the boundary. The remaining field vectors ( $E^n$ ,  $H^n$ ,  $D^t$ , and  $B^t$ ) are computed from the constitutive equations  $D = \epsilon E$ , and  $B = \mu H$ .

Using the electric and magnetic fields, the total field energy per unit of length is computed using the equations:

$$W_e = \frac{1}{2} \int EDdA = \frac{1}{2} \int \epsilon E^2 dA \quad W_m = \frac{1}{2} \int BHdA = \frac{1}{2} \int \mu H^2 dA$$

The circuit shunt capacitance matrix per unit of length is computed using the equations:

$$C_{ii} = W_e^i / v^2 \quad \text{and} \quad C_{ij} = (W_e^i + W_e^j - W_e^{ij}) / 2v^2$$

and the circuit series inductance matrix per unit of length is computed using the equations:

$$L_{ii} = W_m^i / i^2 \quad \text{and} \quad L_{ij} = (W_m^i + W_m^j - W_m^{ij}) / 2i^2$$

where  $C_{ii}$ ,  $L_{ii}$  are the matrix diagonal terms,  $C_{ij}$ ,  $L_{ij}$  are the off-diagonal terms, and:

$W_e^i$  is the total electric field energy with a unit charge applied to conductor  $i$

$W_e^{ij}$  is the total electric field energy with a unit positive charge applied to conductor  $i$  and a negative unit charge applied on conductor  $j$ .

$W_m^i$  is the total magnetic field energy with a current  $i$  applied to conductor  $i$

$W_m^{ij}$  is the total magnetic field energy with a current  $i$  applied to conductor  $i$  and a current  $-i$  applied to conductor  $j$ .

Note that while the capacitance equations are linear, the inductance equations are nonlinear since the magnetic permeability inside steel depends on the magnetic flux density. Therefore, the inductance matrix is computed iteratively using *Newton's method*.

Finally the series resistance and shunt conductance matrices are computed based on the conductor (and if present semiconductor) geometry and the material conductivities. Using these matrices the admittance matrix of the entire circuit at a specific frequency is computed using *eigenvalue analysis* based method.

### I. MODEL VALIDATION

The capacitance and inductance computations described above were first checked using analytically derived results for a simple 3-Phase circuit illustrated in Figure 5. The finite element and analytically computed inductance matrix for this system is shown in Figure 5.

The model was subsequently validated with a series of full scale tests performed on a number of specific test circuits. Each test circuit was 100 feet long consisting of ten sections of steel raceway enclosed power circuits. A total of 14 test circuits were tested. The circuits are listed in Table 1. The test

arrangement is pictured in Figure 6. Each circuit was installed on wood beams to avoid contact with the concrete floor.

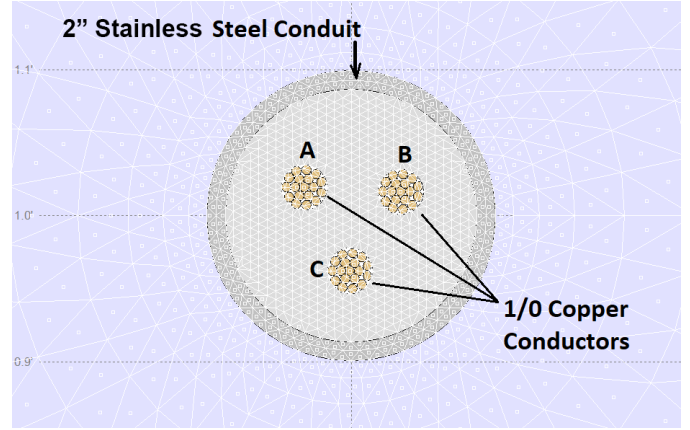


Figure 4: Analytic Validation Circuit Cross-Section

Inductance Matrix ( $\mu\text{H/m}$ ) - FEM Result				
	A	B	C	Raceway
A	0.83877	0.49739	0.49997	0.41722
B	0.49739	0.83872	0.50299	0.41722
C	0.49997	0.50299	0.83879	0.41722
Raceway	0.41722	0.41722	0.41722	0.40685

Analytic Result				
	A	B	C	Raceway
A	0.79938	0.45926	0.46179	0.40612
B	0.45926	0.79938	0.46473	0.40612
C	0.46179	0.46473	0.79938	0.40612
Raceway	0.40612	0.40612	0.40612	0.40612

Figure 5: FEM & Analytic Computation Results

Table 1: List of Steel Raceway Enclosed Power Circuits

#	Raceway	Phase	Neutral	EGC	Test Current (Amperes)
1	EMT ¾"	#8 Cu	#8 Cu	#10 Cu	40/160/320
2	IMC ¾"	#8 Cu	#8 Cu	#10 Cu	40/160/320
3	GRC ¾"	#8 Cu	#8 Cu	#10 Cu	40/160/320
4	EMT 1"	#4 Cu	#4 Cu	#8 Cu	80/240/480
5	IMC 1"	#4 Cu	#4 Cu	#8 Cu	80/240/480
6	GRC 1"	#4 C	#4 Cu	#8 Cu	80/240/480
7	St.Stl 1"	#4 C	#4 Cu	#8 Cu	80/240/480
8	EMT 2"	3/0 C	3/0 Cu	#6 Cu	200/800/1600
9	IMC 2"	3/0 C	3/0 Cu	#6 Cu	200/800/1600
10	GRC 2"	3/0 C	3/0 Cu	#6 Cu	200/800/1600
11	EMT 3"	500kcm	500kcm	#3 Cu	350/1400/2800
12	IMC 3"	500kcm	500kcm	#3 Cu	350/1400/2800
13	GRC 3"	500kcm	500kcm	#3 Cu	350/1400/2800
14	St.Stl 3"	500kcm	500kcm	#3 Cu	350/1400/2800

The instrumentation is conceptually shown in Figure 7. Note that the current in the various conductors of the arrangement is measured with high precision sampling resistors. The temperature of the raceway was also measured at the middle of the first three 10-foot sections. The data was digitized and stored in the computer for post processing.

It is impossible to include all the results in this paper. The reader is referred to the full report [2]. Here we present two

example results with comparison to computer model results. Table 2 shows the measured and computed current split in a conduit-enclosed circuit containing insulated #4-copper phase & neutral conductors and a bare #8-copper equipment grounding conductor. Note that there is good agreement between measured and computed currents.



Figure 6: Photograph of the Experimental Setup

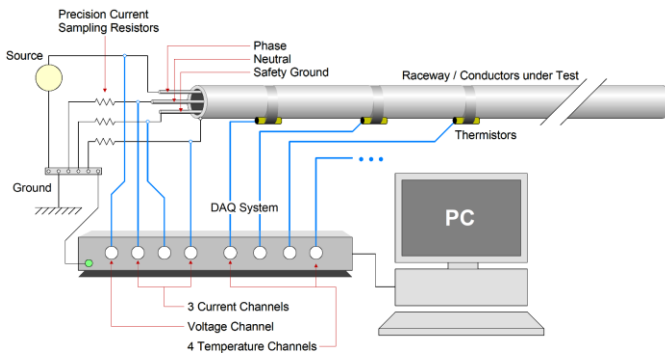


Figure 7: Testing Instrumentation

Table 2: 1"EMT Tests with #4 Copper Phase & Neutral and #8 Equipment Grounding Conductors

Test #		1	2
Applied Voltage (V)		7.630	27.12
Temp ( $^{\circ}$ C)		29.78	33.84
Total Current		155.2	466.4
Neutral Current	Measured	88.40 A	269.6 A
	Computed	89.95 A	264.2 A
Conduit Current	Measured	31.36 A	96.15 A
	Computed	32.16 A	99.90 A
Ground Current	Measured	36.56 A	101.2 A
	Computed	36.09 A	106.1 A

Table 3 shows the measured and computed circuit impedance of 1"EMT containing a single insulated #4 copper conductor. The total circuit impedance decreases with increasing current.

Table 3: 1"EMT Tests with #4 Copper Phase Conductor

Test #	1	2	3
Applied Voltage (V)	9.859	22.45	28.69
Total Current	82.27	237.6	311.4
Temp ( $^{\circ}$ C)	27.05	28.61	33.49

Impedance Magnitude	Measured	120.0	94.5	92.1
	Computed	98.36	93.6	91.1
Impedance Phase	Measured	24.5	23.0	21.1
	Computed	28.18	25.1	22.1

#### IV. APPLICATIONS

The model is used in many different applications. Here we discuss the following: (a) determination of saturation levels in the steel; (b) determination of maximum allowable length of a circuit; (c) effect of current magnitude on conduit impedance; and (d) raceway voltage under fault conditions.

*A. Steel Saturation Levels.* Magnetic saturation in steel raceways results in increased losses and heating of the raceway and the enclosed circuit. The developed model provides the magnetic field level at every point of the raceway and for specific electric current through the circuit. Figure 8 illustrates the performance of 1-inch EMT with a L1-L2-N-G configuration (two #4Cu phase conductors, a #6Cu neutral conductor and a #8Cu equipment grounding conductor). During a L1-L2 fault the current is 4 kA. The plots show the magnetic field intensity (H), the magnetic field flux density (B), and the relative permeability of the material around the raceway circumference. Note that the field peaks at two points corresponding to the closest locations to the phase conductors (at 216 and 316 degrees). Note also the raceway material saturates at different levels around the circumference.

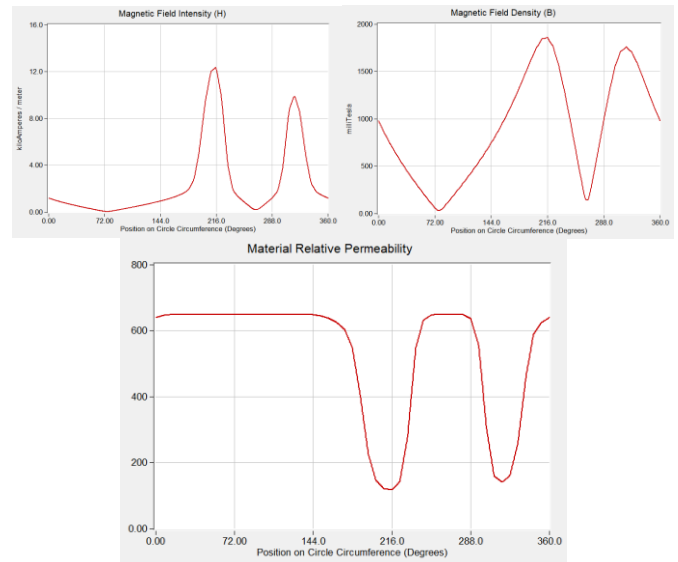


Figure 8: Magnetic Field Intensity (H), Flux Density (B) for and material permeability during 4kA (L1-L2)

*B. Maximum Allowable Length.* The maximum allowable length for a specific system is defined as the maximum length of a circuit which will allow the safe and reliable operation of the overcurrent protective device. The traditional practice is to require that the fault current is above 500% of protective device rating for a fault at the end of the circuit under worst conditions of a 50 V arc voltage. The fault current depends on

the system impedance, fault arc voltage, and return path impedance. The return path may be a combination of paths, such as steel conduit or tubing, equipment grounding conductor, neutral, earth, etc. The worst condition is one that will result in maximum impedance for the fault path. Consider the simple circuit of Figure 9. For a single phase-to-ground conductor fault (*LI-G*), the fault current return path is through the parallel combination of the equipment grounding conductor and the raceway assuming that the neutral (which is not shown in the figure) is grounded at one location only.

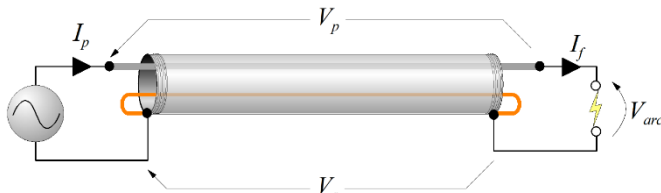


Figure 9: A Simple Faulted Circuit

In general, the arc impedance is purely resistive. In this case, the arc voltage is in-phase with the circuit current, as illustrated in Figure 10.

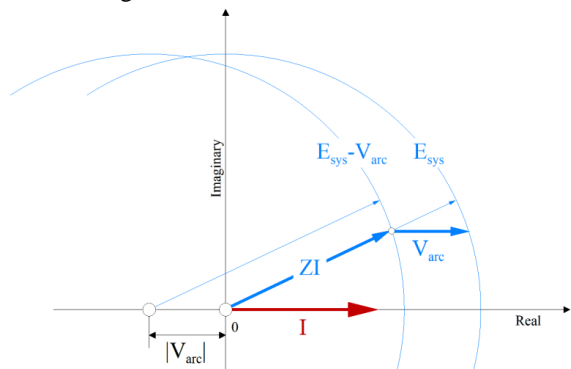


Figure 10: Phasor Illustration During a Fault

The phasor equation describing this condition is as follows:

$$E = V_{arc} + IZ\ell$$

Splitting the above in phasors that are in-phase with the current and those perpendicular to the current and taken the absolute value of the resulting equation we obtain:

$$E^2 = (V_{arc} + IR\ell)^2 + (IX\ell)^2$$

Above equation is solved for the length, yielding:

$$\ell = \frac{-V_{arc}R + \sqrt{V_{arc}^2R^2 + Z^2(E^2 - V_{arc}^2)}}{IZ^2}$$

Similar equations can be derived for any type of fault and arc voltage. The source voltage is assumed to be the rated source voltage because for almost all applications, the source impedance is assumed to be small compared to the circuit impedance. The permissible length is computed by using a fault current value of 500% of protective device rating and a 50V arc voltage. Table 4 provides typical results obtained with the model. These results are more accurate than comparable results provided in the NEC and the Soares book on grounding. Table 5 provides similar results for stainless steel conduit.

Table 4: Maximum Permissible Circuit Length (50V arc voltage and current 500% of protective device rating, Conductors at 75°C, Raceways at 30°C, LC1: line-to-raceway fault)

Raceway Size inches	Conductor Size	Over-current Device Rating Amps	Max Length of Raceway Run (feet)			
			Soares 13th Edition	Computed by GEMI Program		
				EMT	MC	GRC
½	#12	20	350	214	228	228
	#10	30	345	185	201	201
¾	#10	30	355	222	227	224
	#8	50	315	173	178	175
1	#8	50	335	203	203	203
	#4	85	266	185	184	184
1 ¼	#2	115	265	203	190	190
1 ½	#1	130	265	212	201	200
	2/0	175	220	182	172	170
2	3/0	200	255	199	189	188
	4/0	230	230	183	175	172
2 ½	250 kcm	255	265	217	194	189
	350 kcm	310	235	194	177	169
3	500 kcm	380	230	194	176	169
	600 kcm	420	230	183	168	159
3 ½	700 kcm	460	230	199	171	163
	800 kcm	490	230	192	166	156
4	900 kcm	520	235	199	171	161
	1000 kcm	545	235	193	167	157
5	1500 kcm	625	245	N/A	N/A	162
	1750 kcm	650	240	N/A	N/A	159

Table 5: Maximum Permissible Circuit Length for Stainless Steel (50V arc voltage and current 500% of protective device rating, LC1: line-to-raceway fault)

Raceway Size (inches)	Conductor Size	Over-current Device Rating Amperes	Max Length of Steel Raceway Run (feet)
½	#12	20	204
	#10	30	174
¾	#10	30	201
	#8	50	150
1	#8	50	153
	#4	85	122
1 ¼	#2	115	166
1 ½	#1	130	178
	2/0	175	146
2	3/0	200	169
	4/0	230	153
2 ½	250 kcm	255	207
	350 kcm	310	181
3	500 kcm	380	186
	600 kcm	420	172
4	900 kcm	520	204
	1000 kcm	545	198

5	1500 kcm	625	221
	1750 kcm	650	216

C. *Effect of Electric Current Magnitude on Raceway Impedance.* Because of the nonlinear characteristics of the steel raceway, the impedance is dependent upon the electric current magnitude and current distribution among the alternate paths (phase conductors, neutrals, equipment grounding conductors and the raceway). Specifically, as the electric current magnitude increases, the steel raceway is driven to higher levels of “saturation,” which causes a reduction of the steel raceway impedance. The phenomena are complex because the saturation of the steel raceway is not uniform. In addition, the saturation level and pattern depends on the way the current carrying conductors are placed in the raceway. For a specific configuration the proposed model will provide the overall impedance of the circuit. As examples we present in Table 6 the computed total circuit impedance for several circuits considering the simple configuration of one single insulated conductor (insulation thickness of 70 mils) resting on the inside of the raceway and the current returning through the raceway.

**Table 6: Steel Raceway Circuit Impedance vs Current**

#	Raceway	Phase Cond.	Current (A)	mΩ for a 100 foot Circuit	
				Resistance	Reactance
1	EMT ¾	#8 Cu	50	164	53.2
			100	162	52.0
			400	158	28.3
2	IMC ¾	#8 Cu	50	156	54.4
			100	155	54.2
			400	151	42.4
3	GRC ¾	#8 Cu	50	159	57.7
			100	158	55.8
			400	154	42.1
4	EMT 1"	#4 Cu	100	91.4	46.8
			300	86.7	34.5
			1200	85.5	16.1
5	IMC 1"	#4 Cu	100	88.1	46.5
			300	84.5	43.0
			1200	82.1	23.6
6	GRC 1"	#4 Cu	100	88.0	50.1
			300	85.0	44.6
			1200	82.4	28.6
8	EMT 2"	3/0 Cu	500	33.8	23.3
			1200	32.8	14.9
			4800	32.5	9.01
9	IMC 2"	3/0 Cu	500	35.0	26.5
			1200	32.5	20.9
			4800	31.6	11.6
10	GRC 2"	3/0 Cu	500	34.6	27.7
			1200	32.5	22.2
			4800	31.7	15.8
11	EMT 3"	500kcm	2000	16.8	11.1
			4000	16.7	8.55
			16000	16.7	6.50
12	IMC 3"	500kcm	2000	15.8	17.7
			4000	14.7	13.2
			16000	14.2	8.82
13	GRC 3"	500kcm	2000	16.6	18.5

		4000	15.7	15.5
		16000	15.1	12.9

D. *Raceway Voltage under Fault Conditions (Ground Potential Rise of Steel Raceway).* During normal operation of the system, the steel raceway voltage is very low and it is safe for humans to touch it. During faults, the voltage of the steel raceway or any grounded item may be elevated to a substantial voltage. Using the developed model, an investigation was performed of the steel raceway/ground voltage during faults. For this investigation, the simple system of Figure 11 was utilized. The system comprises a section of overhead medium voltage distribution circuit, a 13.8kV/480V transformer, a 480V raceway enclosed circuit, a 7.9kV/120V single phase transformer and two 120V raceway enclosed circuits. Faults on the utility side, as well as on the secondary distribution system, were studied. Typical results are presented in Figures 11a, 11b and 11c.

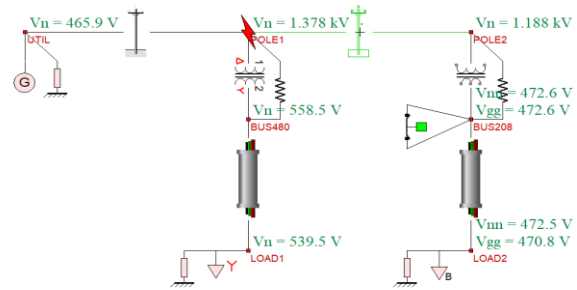


**Figure 11a: Example Test System for GPR Computations – Ground Fault on 13.8 kV System**

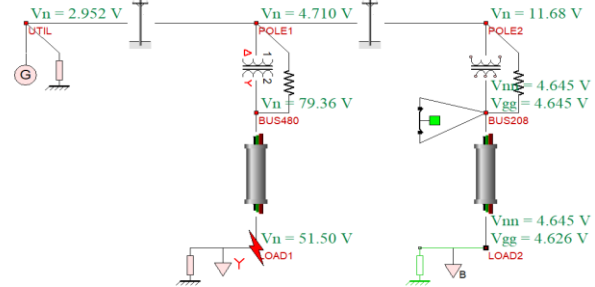


**Figure 11b: Example Test System for GPR Computations – Ground Fault on 480 V System**

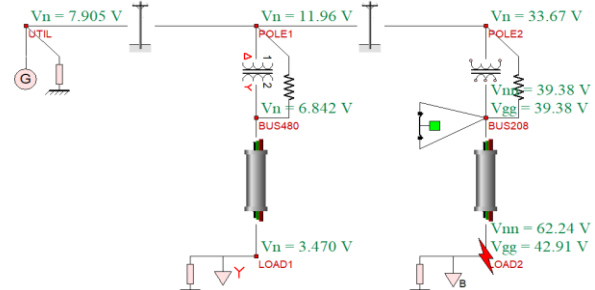


**Figure 11c: Example Test System for GPR Computations – Ground Fault on 120 V System**

The figures indicate the location of the ground fault as well as the ground potential rise on the neutral conductors and equipment grounding conductors of the system. The results

support the following conclusions: (1) the ground potential rise during ground faults in the secondary circuit is a portion of the operating voltage; for 120-V systems, the calculated voltages are below permissible values, as dictated by standards such as the IEEE Std 80, (2) the ground potential rise of steel raceways during ground faults on the utility side may be quite high; as a matter of fact, a big portion of the utility ground potential rise is transferred to the steel raceway.

## V. SUMMARY AND DISCUSSION

A comprehensive and high fidelity model of steel raceway enclosed power circuits has been developed which computes electric field and magnetic field distributions. Current splits among the various paths based on the impedance of the steel raceway with enclosed power conductors. The model is capable of predicting the effect of temperature and electric current levels on the total impedance and the level of magnetic saturation of the steel raceway. The model has been validated with extensive full scale test results and a method to measure the material parameters of the various steel materials used for raceways. The model can be used for a number of applications. Example results have been presented of: (1) saturation patterns and levels in the steel; (2) maximum allowable length of a circuit; (3) effects of current magnitude on raceway impedance; and (4) ground potential rise in raceways, neutral conductors and equipment grounding conductors under various fault conditions.

## REFERENCES

- [1] A. Meliopoulos, Elias Glytsis, Richard Loyd, and Patricia Horton, "Performance Evaluation of Steel-Conduit-Enclosed Power Systems," in *IEEE Transactions on Industry Applications*, Vol 35, No. 3, pp 515-523, May-June 1999.
- [2] Jianming Jin, "The Finite Element Method in Electromagnetics", 2<sup>nd</sup> Edition, 2002.
- [3] R. H. Kaufmann, "Let's be more specific about equipment grounding," in *Proc. American Power Conf.*, 1962, pp. 913-922.
- [4] A. Meliopoulos, G. J. Cokkinides, and G. K. Stefopoulos, "Quadratic integration method," in *Proceedings of the 2005 International Power System Transients Conference (IPST 2005)*, 2005, pp. 19-23: Citeseer.
- [5] Hairer, Ernst, Syvert Paul Nrssett, and Gerhard Wanner. Solving Ordinary Differential Equations: Nonstiff problems. v. 2: Stiff and differential-algebraic problems. Springer Verlag, 1996 .pp.75-77.
- [6] National Electrical Code.
- [7] National Electrical Safety Code.
- [8] IAEI, The Soares Book on Grounding, 9th Edition.
- [9] FIPS PUB 94: Guideline on Electric Power for ADP Installations, Sept 1983.
- [10] ANSI/IEEE Std 80, IEEE Guide for Safety in AC Substation Grounding, 1986.
- [11] IEC 479-1: Effects of Current Passing Through Human Body, 1984.
- [12] ANSI/IEEE Std 81, IEEE Guide for Measuring Earth Resistivity, Ground Impedance and Earth Surface Potentials of a Ground System.
- [13] IEEE 519-1992 Standard. Harmonics in Power Systems, IEEE New York, NY
- [14] IEEE 1100-1999 Standard, Emerald Book, IEEE New York, NY
- [15] IEEE Std 142-1991, IEEE Recommended Practice for Grounding of Industrial and Commercial Power Systems.
- [16] IEEE Std 487, IEEE Guide for Protection of Wire-Line Communication Facilities Serving Electric Power Stations.
- [17] IEEE Std 837, IEEE Standard for Qualifying Permanent Connections Used in Substation Grounding.

- [18] IEEE Std 1048-1990, IEEE Guide for Protective Grounding of Power Lines.
- [19] IEEE Std 1584-2002, IEEE Guide for Performing Arc-Flash Hazard Calculations
- [20] Modeling and testing of steel EMT, IMC, and RIGID (GRC) conduit," Georgia Inst. Technol. Atlanta, GA, May 1994.
- [21] J. P. Simmons, *The Soares Book on Grounding*, 4th ed., Int. Assoc. Elect. Inspectors, Park Ridge, IL, 1990.
- [22] A. P. Meliopoulos, *Power System Grounding and Transients: An Introduction*. New York: Marcel Dekker, 1988.
- [23] S. Schaffer, "Minimum sizing of equipment grounding conductor," *EC&M Mag.*, pp. 78-82, Aug. 1991.
- [24] A. P. Meliopoulos, *Standard Handbook for Electrical Engineers, Section 27, Lightning and Overvoltage Protection*, 13th ed. New York: McGraw-Hill, 1993.
- [25] A. P. Meliopoulos and M. G. Moharam, "Transient analysis of grounding systems," *IEEE Trans. Power App. Syst.*, vol. PAS-102, pp. 389-397, Feb. 1983.
- [26] A. P. Meliopoulos, R. P. Webb, E. B. Joy, and S. Patel, "Computation of maximum earth current in substation switchyards," *IEEE Trans. Power App. Syst.*, vol. PAS-102, pp. 3131-3139, Sept. 1983.
- [27] A. D. Papalexopoulos and A. P. Meliopoulos, "Frequency dependent characteristics of grounding systems," *IEEE Trans. Power Delivery*, vol. PWRD-2, pp. 1073-1081, Oct. 1987.
- [28] G. J. Cokkinides and A. P. Meliopoulos, "Transmission line modeling with explicit grounding representation," *Elect. Power Syst. Res.*, vol. 14, no. 2, pp. 109-119, Apr. 1988.
- [29] A. P. Meliopoulos and J. F. Masson, "Modeling and analysis of URD cable systems," *IEEE Trans. Power Delivery*, vol. 5, pp. 806-815, Apr. 1990.
- [30] A. P. Sakis Meliopoulos and M. A. Martin, Jr., "Calculation of secondary cable losses and ampacity in the presence of harmonics," *IEEE Trans. Power Del.*, vol. 7, pp. 451-459, Apr. 1992.
- [31] A. P. Sakis Meliopoulos, F. Xia, E. B. Joy, and G. J. Cokkinides, "An advanced computer model for grounding system analysis," *IEEE Trans. Power Del.*, vol. 8, pp. 13-23, Jan. 1993.

## II. APPENDIX A: STEEL MATERIAL PARAMETER MEASUREMENTS

The permeability measurement for IMC, EMT and GRC materials was performed using samples of IMC, EMT and GRC conduits listed in Table A-1. Two windings were added on each sample, specifically, a primary winding distributed along the complete circumference, and a concentrated secondary winding. Figure A-1 shows the sample dimensions as well as examples of samples with the added windings. The primary winding was driven by a sinusoidal voltage source. The primary RMS winding current and the secondary RMS winding voltage were measured at various current amplitudes, and the permeability parameters were derived from these measurements. The overall lab setup is shown in Figure A-2.

**Table A-1: Raceway Sample Dimensions**

Material	Size	Outside Diameter (inches)	Width (inches)	Height inches	Turns Prim/Sec
EMT	2"	2.20"	0.068"	2.25"	84/20
IMC	2"	2.36"	0.111"	1.83"	88/20
GRC	2"	2.38"	0.145"	2.03"	90/20
Stainless Steel RMC	1"	1.33"	0.138"	1.347"	44

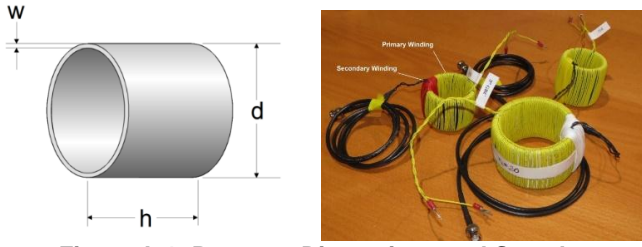


**Figure A-1: Raceway Dimensions and Samples**

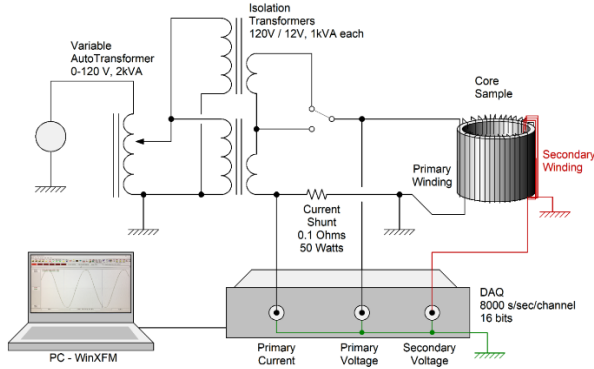


**Figure A-2: Lab Setup**

The magnetic field intensity  $H$  is computed from the measured RMS current using the equation:

$$H_{RMS} = \frac{N_1}{\pi(d-a)} I_{RMS} \sin(\theta)$$

where  $N_1$  is the number of primary turns and  $\theta$  is the phase angle between voltage and current. The magnetic flux density  $B$  is computed from the measured RMS voltage using the equation:

$$B = \frac{V}{N_2 ab \omega}$$

where  $N_2$  is the number of secondary turns and  $\omega$  is the excitation frequency. Note also that:

$$v(t) = \frac{d}{dt} \lambda(t) = \frac{d}{dt} \frac{ab \mu_0 \mu_{rel} N_1 N_2 i(t)}{\pi(d-a)}$$

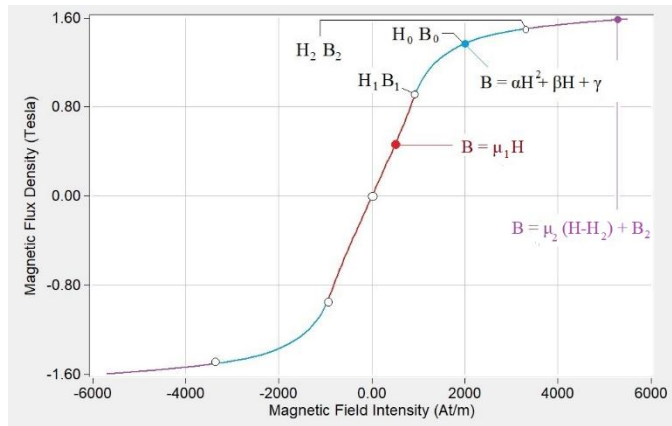


**Figure A-3: Piece-wise linear/quadratic BH curve**

Assuming sinusoidal conditions, and converting to the frequency domain:

$$V = \frac{\omega ab \mu_0 \mu_{rel} N_1 N_2 I}{\pi(d-a)} \quad \text{Or:} \quad \mu_{rel} = \frac{\pi(d-a)V}{\omega ab \mu_0 N_1 N_2 I}$$

The above equation is used to compute the material permeability before saturation onset. Subsequently, multiple measurements were taken by increasing the excitation current to levels that ensured magnetic material saturation. The collected data were analyzed using a time domain model. The saturation curves were derived by minimizing the RMS error between measurement and model results. The saturation curves were expressed in terms of piece-wise linear/quadratic functions as illustrated in Figure A-3. This approach results in a compact representation of the permeability data in terms of the Piece-wise linear/quadratic function parameters.

### III. BIOGRAPHIES

**A. P. Sakis Meliopoulos** (M '76, SM '83, F '93) was born in Katerini, Greece, in 1949. He received the M.E. and E.E. diploma



from the National Technical University of Athens, Greece, in 1972; the M.S.E.E. and Ph.D. degrees from the Georgia Institute of Technology in 1974 and 1976, respectively. In 1971, he worked for Western Electric in Atlanta, Georgia. In 1976, he joined the Faculty of Electrical Engineering, Georgia Institute of Technology, where he is presently the Georgia Power Distinguished Professor,

site director of PSERC and academic administrator of the Power Systems Certificate program. He holds three patents, he has published over 400 technical papers and three books. He received the IEEE Richard Kaufman Award and the George Montefiore Award from the Montefiore Institute, Belgium.

**George Cokkinides** (M '85, SM '05) was born in Athens, Greece, in



1955. He obtained the B.S., M.S., and Ph.D. degrees at the Georgia Institute of Technology in 1978, 1980, and 1985, respectively. From 1983 to 1985, he was a research engineer at the Georgia Tech Research Institute. He served with the faculty of the University of South Carolina from 1985-2000 as Associate

Professor of EE. In 2000 he returned to Georgia Tech. His research interests include power system modeling and simulation, power electronics applications, power system harmonics, and measurement instrumentation.

**Joseph Andre** (A '77, BS '79) is a Technical Consultant for the Steel Tube Institute and an accomplished presenter and instructor in



the electrical field. He received an Associate Degree with Honors from Monroe Community College in Rochester, NY in Business Administration awarded in 1977 and a Bachelor's Degree in Business Administration from the University of Oregon, Eugene, OR, awarded in 1979. Prior to joining STI, Joe worked as a Field Representative for the National Electrical

Manufacturers Association representing over 400 electrical equipment manufacturers. He is a licensed Master Electrician in the state of Washington. Joe Andre presents at over 20 conferences and training session a year on the subject of electrical system design and the National Electrical Code (NEC). Joe has been an Instructor for the National Fire Protection Association on the National Electrical Code since 2012 and an electrical apprenticeship instructor and seminar presenter since 1985.